Available online at www.sciencedirect.com

ScienceDirect

Acta Materialia 81 (2014) 487–500

Acta MATERIALIA

www.elsevier.com/locate/actamat

Deformation mechanisms in an austenitic single-phase duplex microstructured steel with nanotwinned grains

F.K. Yan,[a] N.R. Tao,[a] F. Archie,[b] I. Gutierrez-Urrutia,[b] D. Raabe[b] and K. Lu[a,c,*]

[a] *Shenyang National Laboratory for Materials Science, Institute of Metal Research, Chinese Academy of Sciences, Shenyang 110016, People's Republic of China*

[b] *Max-Planck-Institut für Eisenforschung, Max-Planck Str. 1, D-40237 Düsseldorf, Germany*

[c] *Herbert Gleiter Institute of Nanoscience, Nanjing University of Science & Technology, Nanjing 210094, People's Republic of China*

Received 21 May 2014; revised 26 August 2014; accepted 28 August 2014

Abstract—A novel type of duplex microstructure is generated in a single-phase austenitic steel (AISI 316L; X2CrNiMo19-12), consisting of plastically compliant recrystallized austenitic grains as the matrix containing coarse non-recrystallized grains with a nanotwinned austenitic (*nt*-γ) structure as strengthening inclusions. This novel type of single-phase yet duplex microstructured steel exhibits an excellent combination of strength and ductility. We study the plastic co-deformation mechanisms between the nanotwinned and the recrystallized grains under tension using electron backscatter diffraction (EBSD) and transmission electron microscopy (TEM). At tensile strains below 5%, the *nt*-γ grains nearly deform homogeneously in conjunction with the surrounding statically recrystallized (SRX) grains without generating notable strain localization near their interfaces. The anisotropic plastic deformation of the *nt*-γ grains with predominant shear parallel to the twin boundaries results in a higher dislocation density in the neighboring SRX grains. As the strain exceeds 12%, localized deformation occurs within the *nt*-γ grains in the form of shear banding. A strain gradient is developed in the surrounding SRX grains as a function of distance from the *nt*-γ/SRX interface. Deformation twinning is observed in the SRX grains near the *nt*-γ grains, while away from *nt*-γ grains dislocation slip dominates the deformation. The strengthening effect of the strong and ductile *nt*-γ grains may offer a novel approach to strengthen austenitic steels and related alloys by generating a nanotwinned/recrystallized duplex microstructure.

Keywords: Nano-twinned structures; Austenitic steels; Plastic deformation mechanism; TEM and EBSD characterization

1. Introduction

The development of high-strength steels suffers from a trade-off between strength and ductility [1–3]. For example, in dual-phase (DP) steels, with an increasing fraction of hard martensite phase the strength rises at the expense of ductility [4,5]. Studies on maraging steels showed a similar phenomenon that strength rises significantly due to the formation of nanosized intermetallic precipitates, but their ductility drops markedly [6,7]. The strength–ductility relation, like that in many other metallic alloys, exhibits a typical "banana shaped" inverse trend, i.e., ductility drops more significantly than additional strength is gained [4,7,8]. This phenomenon originates in many multiphase alloys from the incompatibility in plastic deformation between the reinforcing (hard) phase and the (soft) matrix, as well as their interfaces where geometrically necessary dislocations (GNDs) and strain gradients are generated [9–12]. Also, insufficient strain-hardening reserves of the matrix material at higher loads promote such an inverse strength–ductility effect.

Recently, a novel approach was proposed for strengthening metals by means of nanoscale twins [13–16]. Nanotwinned metals and alloys have attracted considerable attention over past years due to their excellent mechanical properties and high thermal stability. The nanotwin strengthening is based on the fact that twin boundaries (TBs) not only are effective in blocking dislocations motion, but also enable dislocation slip and accumulation. Thereby, metals can be strengthened significantly while keeping ductility. For instance, ultrafine-grained Cu films containing nanoscale growth twins exhibit a strength of ~1 GPa with a tensile strain of 13% [17].

With this strengthening mechanism, austenitic steels can be strengthened by means of nanotwinned austenitic grains which are very strong (yield strength comparable to or even higher than martensite) and ductile, with high work-hardening capability [8,18–22]. Recent work in our group has demonstrated the feasibility of producing austenitic duplex-type microstructures in an AISI 316L (X2CrNiMo19–12) stainless steel by means of dynamic plastic deformation (DPD) followed by thermal annealing [18].

* Corresponding author at: Shenyang National Laboratory for Materials Science, Institute of Metal Research, Chinese Academy of Sciences, Shenyang 110016, People's Republic of China.; e-mail: lu@imr.ac.cn

http://dx.doi.org/10.1016/j.actamat.2014.08.054
1359-6462/

The developed duplex-type microstructures consist of nanotwinned austenite (*nt*-γ) grains that are embedded in a matrix of softer recrystallized coarse-grained austenite. The novelty lies in the elastic compatibility of the two types of coexisting microstructures and the idea of using nanotwinned grains as hard inclusions for strengthening. These single-phase duplex microstructured austenite steels exhibit an excellent combination of strength and ductility. For instance, the yield strength can be as high as ~900 MPa while keeping a high uniform ductility (~15%) [18].

In contrast to conventional hard second phases or structures (e.g. carbide, martensite or bainite) to strengthen steels, nanotwinned austenitic grains possess the same elastic modulus as the austenite host matrix and do not create any phase boundary. This means that the single-phase duplex microstructure is more attractive than conventional multi-phase design concepts due to the better elastic and plastic compatibility between the two types of interacting austenitic grains (hard *nt*-γ and soft statically recrystallized (SRX)). Studying the plastic deformation mechanisms associated with such a unique type of single-phase duplex microstructure is crucial for understanding the obtained superior mechanical properties. The present work is thus aimed to reveal the plastic co-deformation mechanisms of the 316L stainless steel strengthened by nanotwinned austenitic grains by using systematic electron backscattered diffraction (EBSD) and transmission electron microscopy (TEM) characterization.

2. Experimental

2.1. Sample preparation

The material studied is a commercial AISI 316L austenitic stainless steel with a composition of Fe–16.42Cr–11.24Ni–2.12Mo–0.02C–0.37Si–1.42Mn–0.011S–0.040P (wt.%). The as-received steel samples are cylinder bars 50 mm in diameter, hot forged and solution-heat-treated at 1200 °C for 1 h. The microstructure is fully austenite with an average size of ~100 μm.

Plastic deformation of the 316L samples was performed on a DPD facility at a strain rate of $10^2 - 10^3\ s^{-1}$ at room temperature. The set-up and processing procedures of the DPD facility are described in Ref. [23]. In the present work, cylinder samples with a diameter of 12 mm and a height of 9 mm were processed to an accumulative strain of $\varepsilon = 1.6$ after multiple impacts with a strain of ~0.1–0.2 in each impact. The deformation strain is defined as $\varepsilon = \ln(L_o/L_f)$, where L_o and L_f are the initial and final thickness of the treated samples, respectively. The as-processed samples were subsequently annealed at 750°C for 45 min prior to water-quenching. Microstructure evolutions and mechanical properties of the as-DPD and the annealed-DPD 316L samples were reported previously [18].

2.2. Tensile tests

Uniaxial tensile tests were performed in an Instron 5848 Micro-Tester system with a strain rate of $5 \times 10^{-3}\ s^{-1}$ at room temperature. A contactless MTS LX 300 laser extensometer was used to measure the sample strain upon loading. Tensile specimens were cut into a dog-bone shape from the annealed disk samples with a gauge section of $5 \times 1.5 \times 1.5\ mm^3$. The annealed samples exhibit a yield strength of 642 MPa and ultimate tensile strength (UTS) of 869 MPa. Their uniform elongation and elongation-to-failure are 24.6% and 46.1%, respectively. Tensile tests were interrupted at various strains ($\varepsilon = 0.5\%, 1.8\%, 5\%, 12\%, 22\%$) for structural analysis (see Fig. 1c).

2.3. Microstructure characterization

Microstructures of the tested samples were examined by using a field emission gun scanning electron microscope (FEG-SEM) FEI Nova NanoSEM 430 and a transmission electron microscope JEOL 2010 operated at 200 kV. The cross-sectional (parallel to the tensile axis) TEM foils were sliced from the tensile samples with different strains using a fine diamond saw and thinned to a thickness of ~30 μm by grinding. The foils were thereafter fixed to Mo rings 3 mm in diameter with a hole of 0.6 mm after punching followed by thinning using double-jet electrolytic polishing in an electrolyte of 8% perchloric acid and 92% alcohol at −15°C.

The texture evolution and development of deformation (orientation) gradients were investigated by means of the EBSD technique. EBSD maps were taken in a 6500F JEOL FEG-SEM equipped with a TSL OIM EBSD system at 15 kV acceleration voltage and working distance of 15 mm. Orientation gradients through multiple grains were analyzed using grain reference orientation deviation (GROD) maps. GROD was calculated as the angular deviation from a reference point having the lowest KAM within a given grain [24,25].

3. Results

3.1. Microstructure of the annealed DPD samples

The microstructure of the annealed DPD samples (750°C for 45 min) is composed of two types of unrecrystallized regions, namely, remaining nanoscale twins in the form of bundles (referred as *nt*-γ grains) and some blocks of dislocation structures (DSs), which are embedded in the matrix of SRX grains (Fig. 1a). The SRX grains constitute ~77.0% of the total volume fraction with an average size of ~2.2 μm. Most of the SRX grains are equiaxed with a weak crystallographic texture (see Fig. 3a). The volume fraction of the DS is ~9.4%. Sizes of most *nt*-γ grains range from several to several tens of micrometers, much larger than that of SRX grains. Statistical TEM measurements indicate that the volume fraction of *nt*-γ grains is $\sim 13.6 \pm 4.1\%$. The average twin/matrix (T/M) lamellar thickness is ~23 nm. High density dislocations exist around deformation TBs, although the dislocation density is reduced significantly in comparison with that in the as-DPD state.

Bright field TEM images (Fig. 1b) showed that most SRX grains are clean and uniform in contrast with very low dislocation densities. Some annealing twins are observed in SRX grains. The interfaces between *nt*-γ grains and SRX grains are clear without detectable dislocations inside the SRX grains near the interfaces.

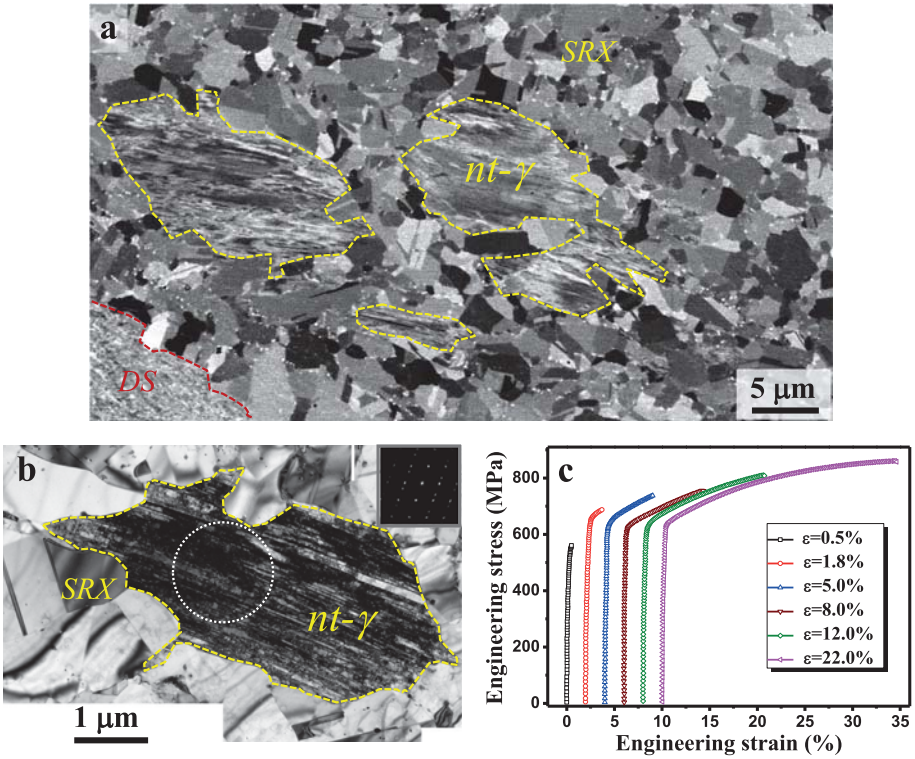

Fig. 1. (a) A typical cross-sectional SEM-ECC image showing *nt-γ* grains (outlined by yellow dotted line) and dislocation structures (DS, outlined by red dotted line) embedded in the static recrystallized (SRX) grains in the annealed-DPD 316L samples at 750°C for 45 min. (b) A typical TEM image of SRX grains embedded with *nt-γ* grains. Inset shows a selected area (circled) diffraction (SAED) pattern of the *nt-γ* grain. (c) Tensile engineering stress–strain curves interrupted to the strain of 0.5%, 1.8%, 5%, 8%, 12% and 22%, respectively. The curves are shifted 2% relative to each other for clarity. (For interpretation of the references to color in this figure legend, the reader is referred to the web version of this article.)

3.2. Plastic deformation of the nanotwinned 316L samples: SEM characterization

3.2.1. SEM–electron channeling contrast (ECC) observations

SEM–ECC images (Fig. 2a and b) show that at the early stages of deformation (true strain $\varepsilon = 1.8$–5%), the SRX grains tend to deform homogeneously. Grain boundaries (GBs) are distinguishable and no pronounced change in the SRX grain sizes is noticed. At $\varepsilon = 12\%$ (Fig. 2c), SRX grains are difficult to be clearly imaged, especially for those close to *nt-γ* grains (arrowed in Fig. 2c). At $\varepsilon = 22.0\%$ (Fig. 2d), SRX grains deformed severely and GBs cannot be distinguished. A shear band (arrowed in Fig. 2d) is found in the *nt-γ* grains, indicative of localized plastic deformation. No cracks or voids are detected in the sample at this strain.

3.2.2. Orientation gradient development

The texture evolution of SRX grains upon tensile deformation was evaluated by EBSD (Fig. 3). The orientation distribution of the SRX grains prior to deformation consists of a brass-type texture with strong brass ({110}<112>) and Goss ({110}<001>) texture components (Fig. 3a). With further straining, these grains develop a β-fiber with strong <111>//TA and <001>//TA components (TA: tensile axis) (Fig. 3b). Texture analysis from EBSD measurements do not reveal any difference in the texture evolution among SRX grains close to *nt-γ* grains and those away from them. Furthermore, coarse *nt-γ* grains contain upon straining similar orientations as those exhibited by finer SRX grains.

Ex situ interrupted tensile tests were conducted to investigate the mechanical compatibility among coarse *nt-γ* grains and fine SRX grains (Fig. 4). As shown the GROD map in Fig. 4a, coarse *nt-γ* grains in the as-processed sample contain orientation gradients which are associated to the high density of crystal defects. Orientation deviation gradients are not visible in those SRX grains surrounding the *nt-γ* grain (Fig. 4a). With straining to 5%, no pronounced orientation deviation is found in the neighboring SRX grains of the *nt-γ* grain, which are located ~2 μm from the interface (outlined in Fig. 4b). Some SRX grains that are located between 2 and 8 μm from the *nt-γ*/SRX interface show slightly higher orientation deviations. Further away from the interface (>8 μm), orientation deviations within SRX grains disappear.

As strain reaches 12% (Fig. 4c), orientation gradients within SRX grains surrounding the *nt-γ* grain/SRX grain interface (~8 μm) become stronger than those occurring within grains further away from the interface. These observations indicate that, due to the mechanical compatibility between the hard coarse *nt-γ* grain and the soft SRX grain, an orientation gradient develops upon straining within the SRX grains close to *nt-γ* inclusion grains. Further increasing the tensile strain to 22% leads to a more homogenous distribution of the orientation gradients inside the SRX grains (Fig. 4d). Additionally, we also found that the GROD values in the SRX grains in the direction of the TA with respect to the *nt-γ* grains is higher than those in

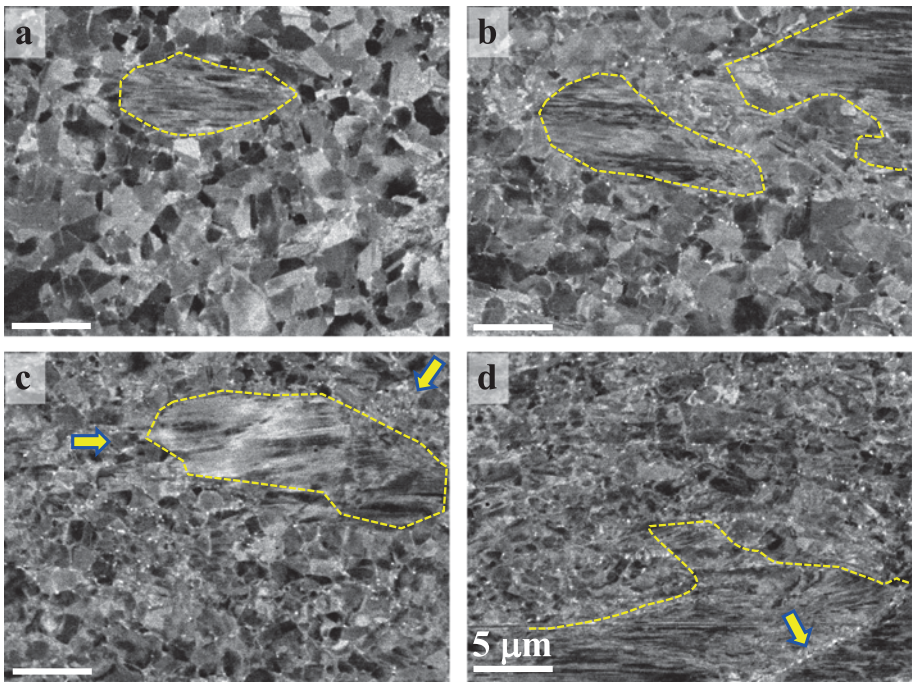

Fig. 2. SEM-ECC images of tensile deformed nanotwinned 316L samples at the strain of: (a) $\varepsilon = 1.8\%$; (b) $\varepsilon = 5\%$; (c) $\varepsilon = 12\%$; (d) $\varepsilon = 22\%$. The arrows in (c) and (d) show the blur SRX grains and the shear band, respectively.

the perpendicular direction. This observation indicates the anisotropic plastic deformation of the *nt-γ* grains.

3.3. Plastic deformation of the nanotwinned 316L samples: TEM characterization

3.3.1. Plastic deformation at low strains (ε = 0.5–5%)

In order to characterize the plastic deformation behavior of SRX grains surrounding the *nt-γ* grains in the nanotwinned 316L samples, large areas of SRX grains with embedded *nt-γ* grains were examined by TEM. The dislocation density in the SRX grains as a function of distance from the SRX/*nt-γ* interface was measured in two directions (vertical and parallel to TBs). The SRX grains are divided into three regions in terms of the distance from the interface, namely, grains adjacent to the *nt-γ* grain (0–2 μm, Region I); grains 2–6 μm away from the SRX/*nt-γ* interface (Region II); and grains > 6 μm away from the SRX/*nt-γ* interface (Region III), as shown in Fig. 5a.

Bright field TEM images showed that in the initial stage of plastic deformation ($\varepsilon = 0.5\%$, Fig. 5a), most SRX grains display uniform contrasts. Some dislocations appear in SRX grains and their density can be measured by counting the number of dislocations in the grains [26]. For comparing the dislocation densities in different SRX grains, most of these grains are tilted to the <1 1 0> or <1 0 0> zone axis so that as many dislocations as possible can be clearly imaged.

As shown in Fig. 6a1–c1, the SRX grains in the direction vertical to TBs were tilted into the <1 1 0> zone axis. Most dislocations are distributed randomly inside the SRX grains. Statistical measurements (Fig. 5b) indicated that the dislocation density in the SRX grains tilted to the <1 1 0> zone axis is in the range $1.0 \sim 4.0 \times 10^{13}\ m^{-2}$ (averagely $2.2 \pm 0.8 \times 10^{13} m^{-2}$) at a strain of 0.5%. For those grains titled to the <1 0 0> zone axis, measured dislocation densities are in the same range as that in the <1 1 0> zone axis with a nearly identical average density ($\sim 2.5 \pm 1.1 \times 10^{13}\ m^{-2}$).

Statistical TEM measurements showed that the dislocation density in Region I along the <1 1 0> zone axis varies around $1.1–3.2 \times 10^{13}\ m^{-2}$, and is $\sim 1.3 - 4.0 \times 10^{13}\ m^{-2}$ for Regions II and III (~10 SRX grains were measured for each region). In the <1 0 0> zone axis, the average dislocation density in Region I is $1.9 \pm 0.9 \times 10^{13}\ m^{-2}$, which is comparable to that in Regions II and III ($2.7 \pm 1.1 \times 10^{13}\ m^{-2}$). Apparently, at a strain of 0.5%, no obvious variation was found for the measured dislocation density in the SRX grains from Region I to Region III. This indicates that the dislocation density in the SRX grains is independent of the distance from the interface in this loading regime. A difference in dislocation densities is also not obvious between the SRX grains surrounding the *nt-γ* grains in the direction vertical to the TBs and in those parallel to the TBs.

As strain increases to 1.8%, the dislocation density in the SRX grains accordingly increases, as shown in Figs. 6a2–c2 and 7a2–c2. At this strain, the dislocation density is too high to be measured by TEM observations. However, from the bright field images we observe that the dislocation densities are roughly comparable in the SRX grains from Region I to III, in both directions (parallel and vertical to the TBs). No clear dislocation gradient is observed in the vicinity of the interface. By comparing Figs. 6a2–c2 and 7a2–c2, we found that more dislocations are generated inside the SRX grains in the direction parallel to the TBs than that vertical to the TBs, indicating a pronounced deformation anisotropy around the *nt-γ* grains. Such a deformation anisotropy may arise from anisotropic deformation of the *nt-γ* grains under tension.

At a strain of 5%, similar dislocation distributions were observed in the SRX grains in both directions as in the sample strained to $\varepsilon = 1.8\%$; however, the dislocation density is evidently higher in the samples strained to 5%, see

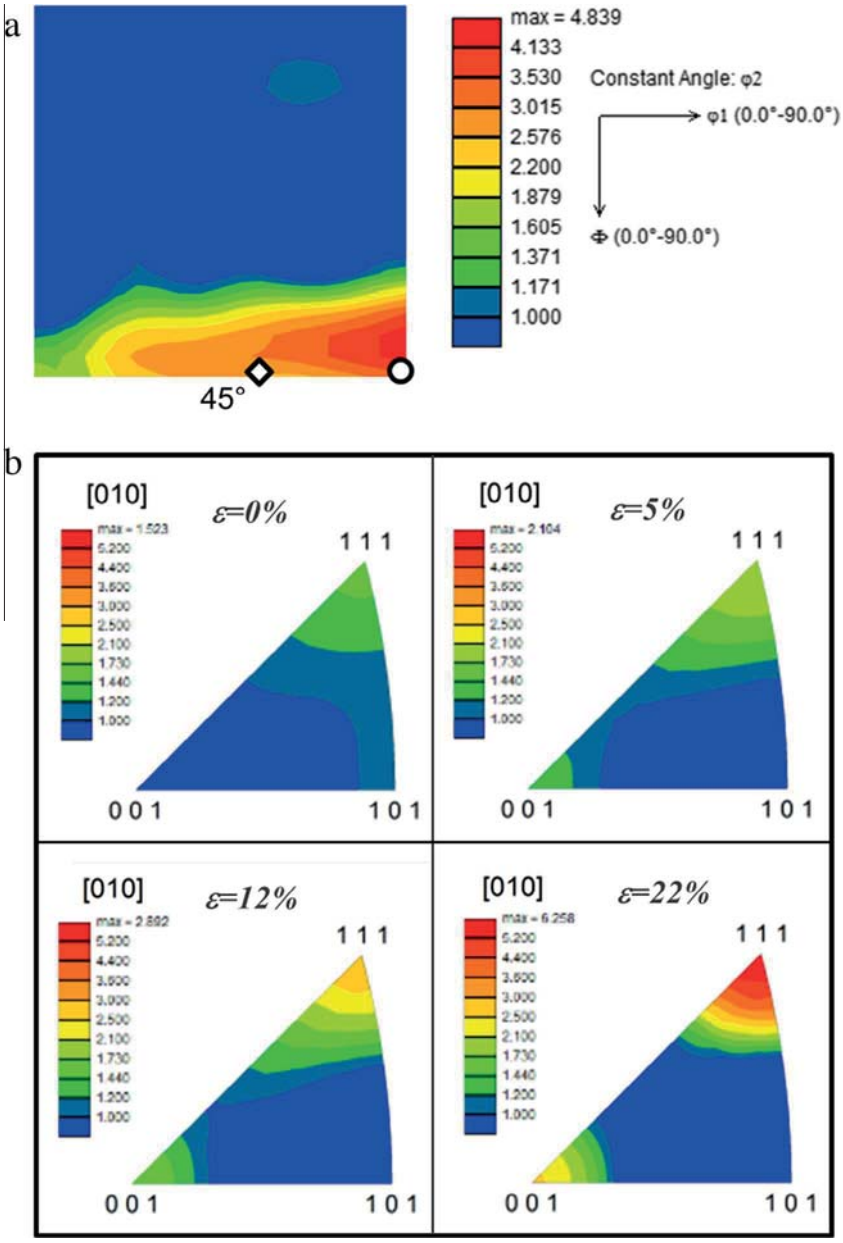

Fig. 3. (a) The orientation distribution function (ODF) map of $\phi_2 = 45°$ section of as-prepared SRX grains. The brass and Goss texture components are shown as diamond and circle in (a), respectively. (b) Inverse pole figures (IPFs) along the TA (corresponding to [010]) direction of SRX grains with straining in the nanotwinned 316L samples.

Figs. 6a3–c3 and 7a3–c3. Dislocation networks are formed in some grains. The dislocation densities near the GBs are much higher than those in the grain interiors (Fig. 7a3–c3). The deformation anisotropy becomes more obvious around the *nt*-γ grains as the dislocation density in the SRX grains parallel to the TBs is much higher than that vertical to the TBs. From a large-area observation (Fig. 8), contrasts of the SRX grains are rather uniform from Regions I to III, without obvious strain gradients near the interface.

3.3.2. Plastic deformation at high strains (ε = 12%–22%)

At a strain of 12%, the dislocation density increases in the SRX grains, forming dislocation cells, walls and tangles, analogous to those observed in conventional deformed metals [27–29]. Dislocations in Region I are arranged forming fine dislocation cells (sizes of 100–300 nm, Fig. 9a). In Regions II and III, dislocation tangles and cells were also observed, but cell sizes are larger (400–1000 nm) than those in Region I, see Fig. 9b. Statistical TEM observations over large areas revealed that the dislocation cell sizes become gradually larger with an increasing distance from the SRX/*nt*-γ interfaces (from Regions I to III).

In addition, in Region I some newly formed deformation twins were detected, see Fig. 10. Detailed observations showed that deformation twins are very thin, a few nanometers thick (Fig. 10b). Interestingly, deformation twinning was activated in those SRX grains located parallel to the active twin system of a coarse *nt*-γ grain. TEM observations do not reveal the activation of deformation twinning in Regions II and III. These observations indicate that plastic

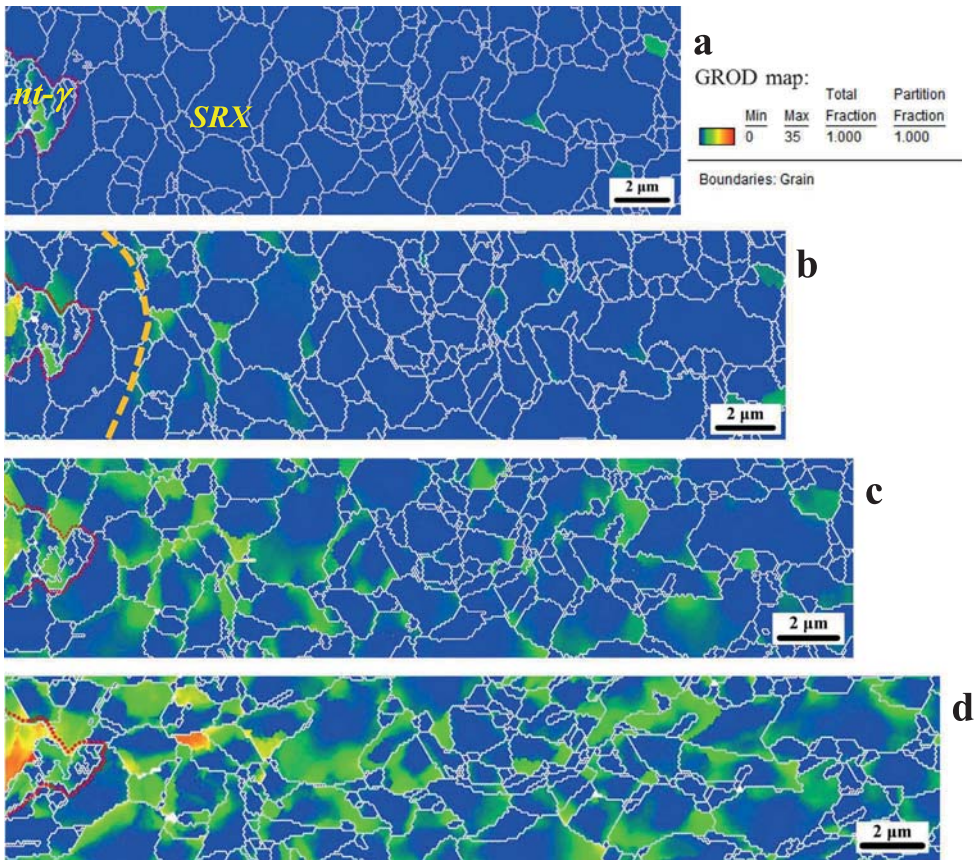

Fig. 4. Orientation gradient distribution based on the GROD map of a typical region consisting of one *nt-γ* grain embedded in a large area of SRX grains in the tensile deformed nanotwinned 316L samples at different strains: (a) $\varepsilon = 0\%$, (b) $\varepsilon = 5\%$, (c) $\varepsilon = 12\%$, (d) $\varepsilon = 22\%$. The neighboring SRX grains (0–2 μm from the interface) of the *nt-γ* grain are outlined by the dashed line.

deformation is more severe in the vicinity of the *nt-γ* grains (Region I) than in Regions II and III.

In the late stage of uniform plastic deformation (22%, prior to necking), we found that deformation twinning occurs in many grains in Region I (arrowed in Figs. 11). At this strain level, SRX grains located perpendicular to the active twin system of a coarse *nt-γ* grain also develop twin substructures. In contrast, in Region III the microstructure still consists of dislocation structures (tangles and cells) without deformation twins. In several SRX grains in Region II, deformation twinning is found occasionally. A gradient variation of the deformation twin density implies local stress concentrations around the SRX/*nt-γ* interfaces.

At a strain of 12%, inhomogeneous deformation of *nt-γ* grains is detected in the form of fine shear bands in the *nt-γ* grains. With further straining to 22%, many *nt-γ* grains are severely deformed by shear banding that cuts the *nt-γ* grains into fragmented pieces in which nanotwinned structures are still visible (Fig. 12). The shear banding regions are characterized by nanosized elongated grains and dislocation cells, similar to those structures observed in Cu–Al alloys [30].

4. Discussion

According to the microstructure characterization, the plastic deformation of the single-phase duplex microstructured nanotwinned 316L material studied here can be divided into two stages, as schematically shown in Fig. 13a–c. In the first stage, homogeneous deformation at small strains (below 5%, Fig. 13b), the *nt-γ* grains co-deform homogeneously without creating noticeable strain gradients with respect to the surrounding SRX grains. In the second stage, inhomogeneous deformation at high strains (12–22%, Fig. 13c), strain gradients are gradually developed within the neighboring SRX grains as a function of distance from the interfaces. This effect leads to deformation twinning inside the SRX grains adjacent to the hard *nt-γ* grains. Localized deformation occurs within the *nt-γ* grains in the form of shear banding. Apparently, the individual intra-grain and the co-deformation mechanisms of the *nt-γ* grains with the abutting *nt-γ*/SRX interface regions are crucial in understanding the plastic deformation of the *nt-γ* grains strengthened 316L steel.

4.1. Plastic deformation of the nt-γ grains

The individual mechanical behavior of the *nt-γ* grains is one of the controlling factors in the plastic deformation of the duplex structure nanotwinned steel. Tensile measurements indicated a very high mechanical strength of ~2.0 GPa for the *nt-γ* grains [18], but their individual ductility is not known yet. It is reported that polycrystalline Cu specimens with nanoscale growth twins produced by electrodeposition exhibits a considerable tensile ductility while possessing an extremely high yield strength [13,17]. The pronounced ductility of the nanotwinned structures was

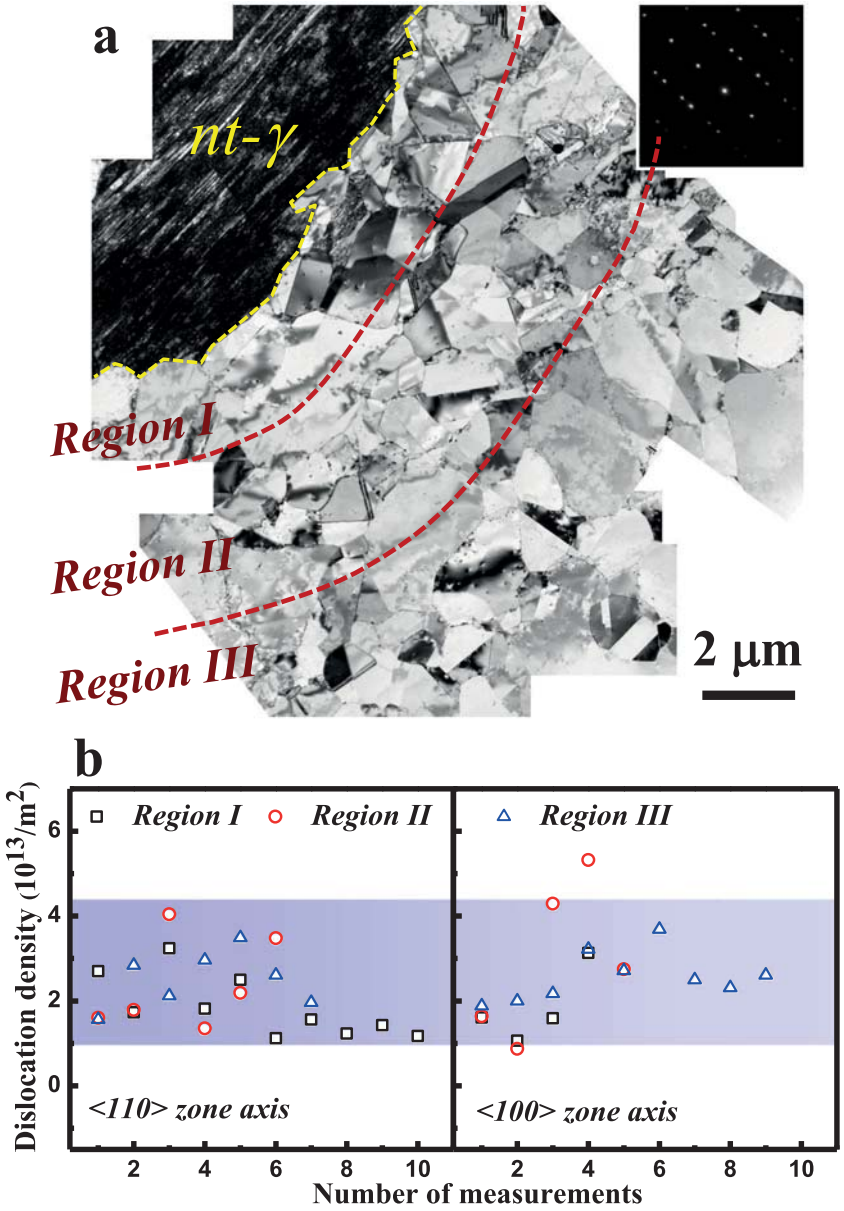

Fig. 5. (a) A typical bright field TEM image of the nanotwinned 316L sample at the strain of 0.5%. SRX grains were divided into three regions along the distance from the interface: Region I (adjacent to the *nt*-γ grain, 0–2 μm away from the interface), Region II (2–6 μm away from the interface) and Region III (more than 6 μm away from the interface). (b) Statistical measurements of dislocation density in SRX grains tilted to the <1 1 0> or <1 0 0> zone axis in different regions.

attributed to a very large density of TBs that enables massive dislocation slip yet suppresses strain localization and strain softening during loading. This mechanism was also revealed by molecular dynamics simulations [31,32] and measurement results which show that the tensile ductility increases significantly with increasing density of TBs (i.e. a decrease of twin/matrix thickness) [17].

However, nanotwinned structures formed via conventional plastic deformation exhibit very limited tensile ductility in Cu [33]. This is attributed to the fact that a very high density of dislocations is generated at TBs during formation of the nanoscale deformation twins. The dislocation densities can be as high as 1.7×10^{16} m^{-2} for the as-DPD Cu [34]. In the subsequent tensile deformation tests, dislocation slip in the nanotwinned structure is then limited by that pre-existing high dislocation density and leaves no reserve for further strain-hardening. Some degree of plasticity can be recovered when the deformation nanotwins are thermally annealed under proper conditions (usually $> 700^{o}$C) during which the dislocation density within the T/M lamellae and at the TBs themselves both decrease considerably. In a recent study [35] it was observed that the dislocation density can be reduced by about one order of magnitude when an as-DPD 316L sample (with a DPD strain of 0.8 and ~60% in volume are nanotwinned) is annealed at 700°C for 30 min. After such recovery annealing, a recovered uniform elongation of 5.2% is achieved in tensile tests of such annealed nanotwinned samples. This means that the nanotwinned grains can after annealing sustain a considerable tensile ductility, due to the thermally induced rearrangement and annihilation of mobile dislocations (e.g., Shockley partials) inside the *nt*-γ

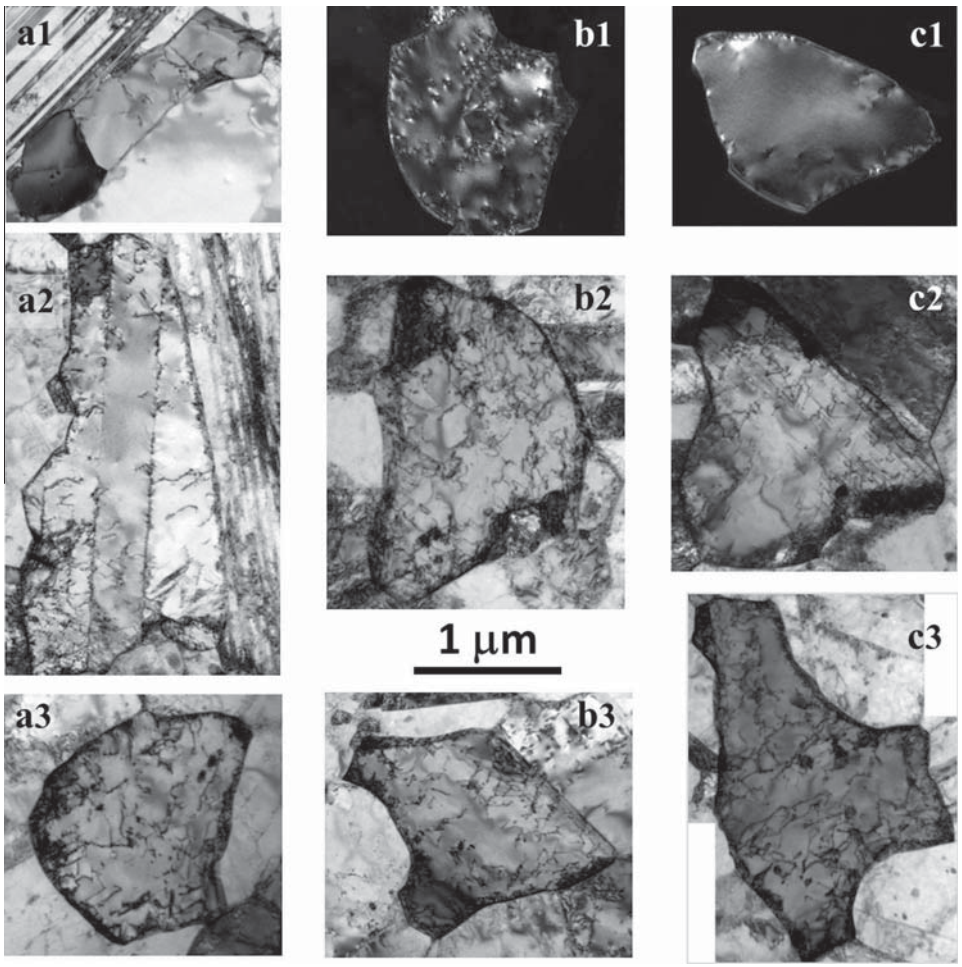

Fig. 6. Typical TEM images of dislocation distribution in SRX grains surrounding the *nt*-γ grains in a direction vertical to TBs in different regions: Region I (a1, a2, a3), Region II (b1, b2, b3) and Region III (c1, c2, c3) at various tensile strains: (a1, b1, c1) 0.5%; (a2, b2, c2) 1.8%; (a3, b3, c3) 5%, respectively. All SRX grains are tilted to the <110> zone axis. (b1) and (c1) are dark-field TEM images for clarity.

grains. Hence, it is reasonable to conclude that the *nt*-γ grains in the annealed DPD 316L samples may regain some capability to accommodate dislocations when exposed to tensile loading, so that they may exhibit a tensile ductility of a few percent with certain work-hardening capability.

The observed difference in dislocation densities in the SRX grains at different positions around the *nt*-γ grains implies anisotropic plastic deformation of the *nt*-γ grains under tension. The higher dislocation density in the SRX grains parallel to TBs than that vertical to TBs indicates that deformation (strain) of the *nt*-γ grains parallel to the TBs is larger than that vertical to the TBs. The anisotropic deformation of the *nt*-γ grains originates from their anisotropic structure and the specific deformation mechanism in the nanotwinned structures. Recent studies [36,37] indicated two hardening modes in nanotwinned structures with different loading directions with respect to the TBs, including hard-mode I (dislocations pile-ups or transfer across TBs) and hard-mode II (threading dislocations motion in the confined T/M lamella). In the present case, the hard-mode II scenario seems to play an important role in the deformation of the *nt*-γ grains during tensile tests, of which the direction is roughly parallel to TBs [19].

When the tensile strain is so large that the stored dislocation density in the *nt*-γ grains is very high and plastic strain of the *nt*-γ grains cannot be accommodated by further dislocation slip and storage, the *nt*-γ grains' ability of dislocation accommodation and work-hardening is exhausted. Then localized deformation is initiated in the *nt*-γ grain to accommodate further plastic strain, as observed in Fig. 12, in the form of shear banding. As systematically investigated earlier [30] in a nanotwinned Cu–Al alloy, shear banding of *nt*-γ grains is an effective approach to accommodate plastic strain, consisting of a nucleation event followed by thickening. Nucleation of a shear band is composed of three steps: (i) initiation of localized deformation (bending, necking and de-twinning) against the T/M lamellae; (ii) evolution of a dislocation structure within the de-twinned band; and (iii) transformation of the de-twinned dislocation structure into a nanosized (sub)grain structure. Thickening of the nucleated shear band with increasing strains proceeds as a transformation process of the adjoining T/M lamellae into the nanosized grain structure analogous to steps (ii) and (iii) of the nucleation process. Our observations in the present nanotwinned 316L steel are consistent with these processes.

4.2. The nt-γ/SRX interfaces and development of strain gradients

In conventional alloys strengthened by a second phase (reinforcement, inclusion), owing to the elastic and/or

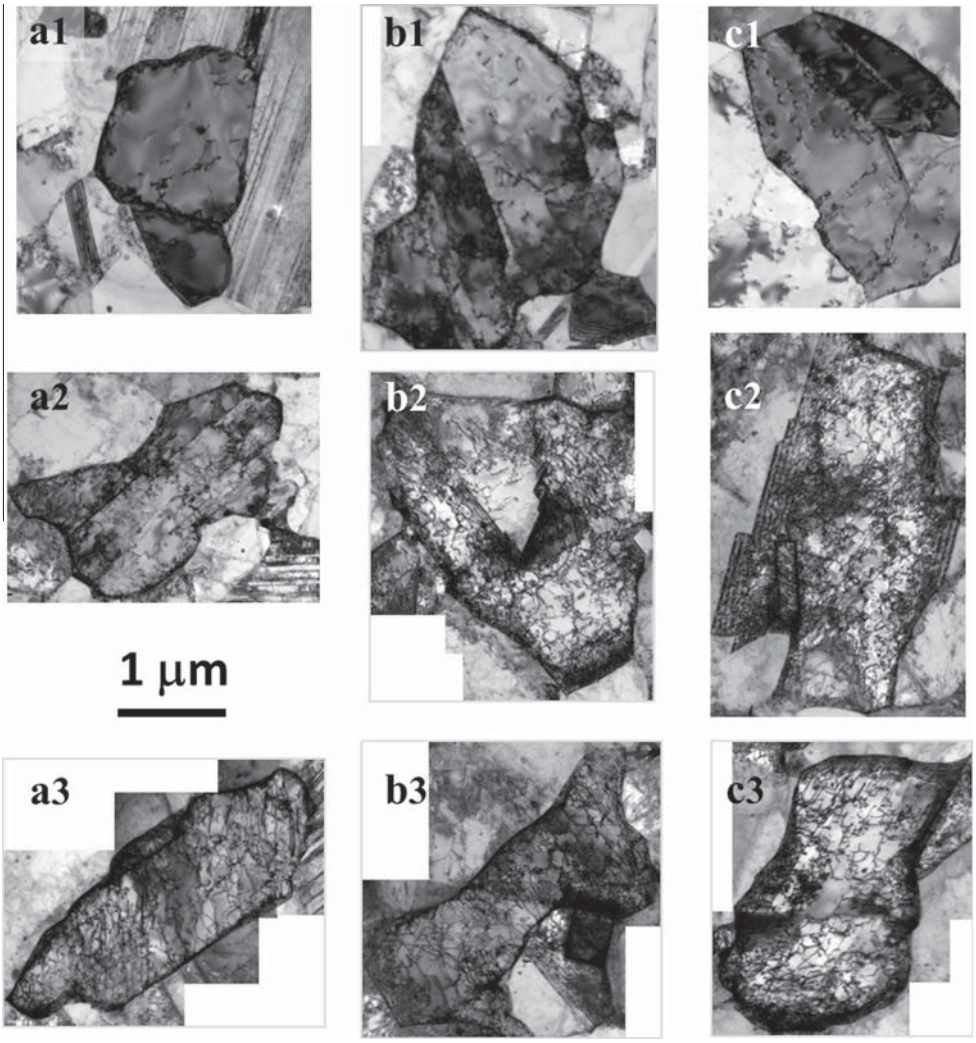

Fig. 7. Typical TEM images of dislocation distribution in SRX grains in a direction parallel to TBs in different regions: Region I (a1, a2, a3), Region II (b1, b2, b3) and Region III (c1, c2, c3) at various tensile strains: (a1, b1, c1) 0.5%; (a2, b2, c2) 1.8%; (a3, b3, c3) 5%, respectively. All SRX grains are tilted to the <1 1 0> zone axis.

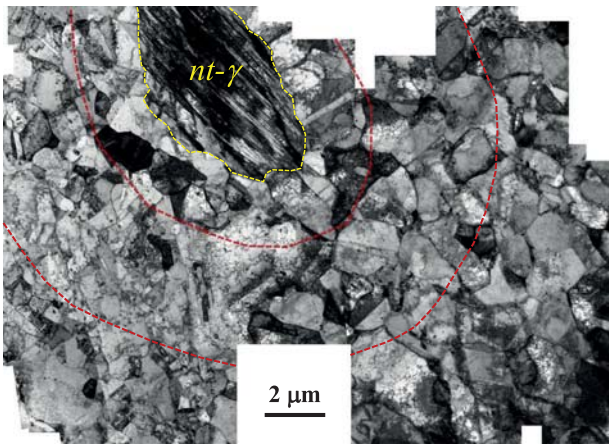

Fig. 8. A TEM image of a *nt*-γ grain and surrounding SRX grains in the nanotwinned 316L samples at the tensile strain of 5%.

plastic mismatch between the reinforcement and matrix, their interfaces are usually preferable sites for dislocation nucleation and hence for strain localization and failure [9,12,38–40]. However, our observations revealed that the interfaces separating the *nt*-γ grains and the SRX matrix grains mechanically behave essentially like conventional iso-phase GBs except for some portions containing TB/GB intersections, see Fig. 14. In the early stage of tension, dislocations nucleate more preferably at the GBs than in the grain interiors. However, no difference is seen at the interfaces and at other SRX GBs regarding dislocation generation. Previous molecular dynamics (MD) simulations showed that Shockley partial dislocations may be preferably nucleated at the TB–GB intersections and glide along TBs within the nanotwinned grains [32]. Nevertheless, this effect is difficult to detect due to the presence of existing high-density dislocations at the TBs in the *nt*-γ grains. A close observation of the TB–GB intersections indicated that they do not act as an active source for dislocation nucleation in the *nt*-γ grains (Fig. 14). Steps or jogs at TBs may also provide possible sites for dislocation nucleation in the *nt*-γ grains [41,42].

As *nt*-γ grains possess some tensile ductility and the interfaces do not seem to act as preferential sites for dislocation generation (Fig. 14), no strain localization will be induced at the interfaces at low strains (below 5%). Hence,

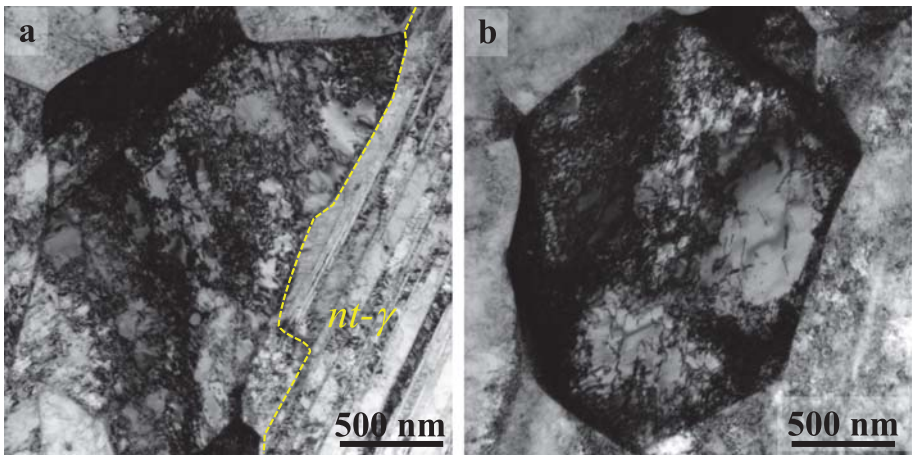

Fig. 9. Typical TEM images of the deformation structures in SRX grains (tilted to the <1 1 0> zone axis) in Region I (a) and Region III (b) at a strain of 12%.

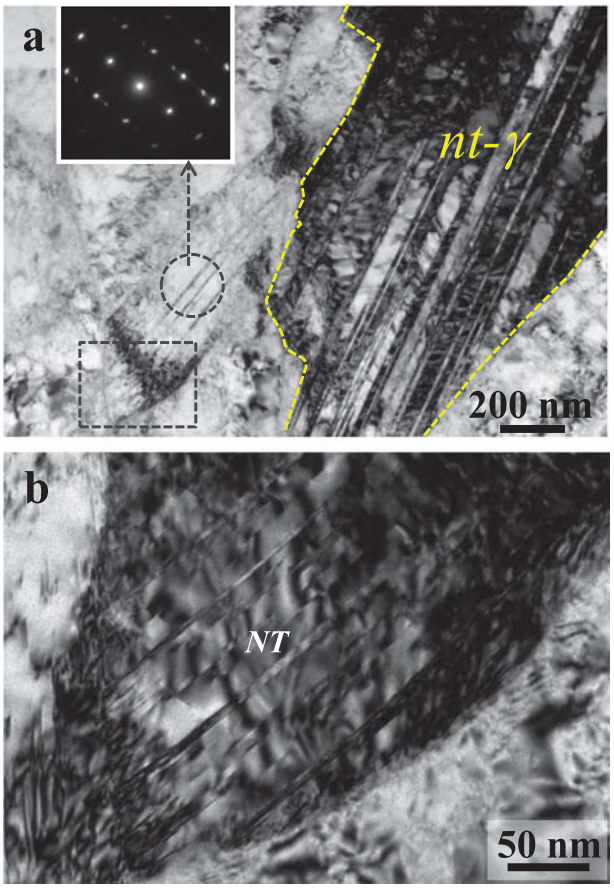

Fig. 10. (a) A typical TEM image showing newly formed deformation twins in the grain roughly in Region I at a strain of 12%. (b) An enlarged image of the region (tilted to the <1 1 0> zone axis) in rectangle in (a). Inset in (a) shows a corresponding SAED pattern of newly formed deformation twins (circled).

homogeneous plastic deformation occurs in the single-phase duplex microstructure consisting of hard *nt-γ* grains embedded in the softer SRX matrix grains. This behavior is distinguished from that in other steels reinforced by hard phases [25,43–45]. For example, in martensite–ferrite DP steels [25,44,45], relatively high geometrically necessary dislocation densities accumulate near the martensite due to the martensitic transformation shear created during cooling after the heat treatment. TEM characterization [44] revealed that the deformation of the ferritic grains or respectively grain clusters is inhomogeneous at different distances from the ferrite–martensite interfaces over the full deformation range when exposed to tensile strains. Higher dislocation densities and/or finer dislocation cell sizes are formed close to the undeformed martensite phase.

Localized deformation of the *nt-γ* grains may unavoidably induce localized stress concentrations at the interfaces and in the adjacent SRX grains, which in turn generates strain gradients. This is verified by observations that deformation twinning occurs in some SRX grains with preferable orientations in the vicinity of *nt-γ* grains at strains above 12% while almost no twinning is found away from the interface (Fig. 10). This evidence indicates that very high stress concentrations can build up around the *nt-γ* grains. It is noted that grain sizes have a pronounced effect on the propensity for deformation twinning during tensile deformation. Larger grain sizes (usually >100 μm) often facilitate deformation twinning [46]. Kashyap and coworkers [27,28] showed that dislocation slip is still a dominant mechanism at a grain size of ~5 μm for 316L at the full range of tensile strains and almost no deformation twinning was found. Hence, deformation twinning in the neighboring grains is ascribed to a very high local stress concentration (high enough for twinning) around the interface. Such a high local stress concentration results from the plastic mismatch strains between the stiff *nt-γ grains* and the softer SRX grains.

At high strains, *nt-γ* grains, analogous to other reinforcing second phases, cannot sustain large uniform deformations together with the SRX grains. This discrepancy in plastic compliance leads to inhomogeneous deformation of nanotwinned samples. Nonetheless, the strain gradients and local stress built up around the interface may be smaller in comparison with that in conventional particle strengthened materials. This is attributed to the localized deformation that can still occur inside the *nt-γ* grains, thereby releasing some of the strain and residual stress [9].

4.3. Work-hardening behavior

According to the well-known Consideré criterion [26,47]:

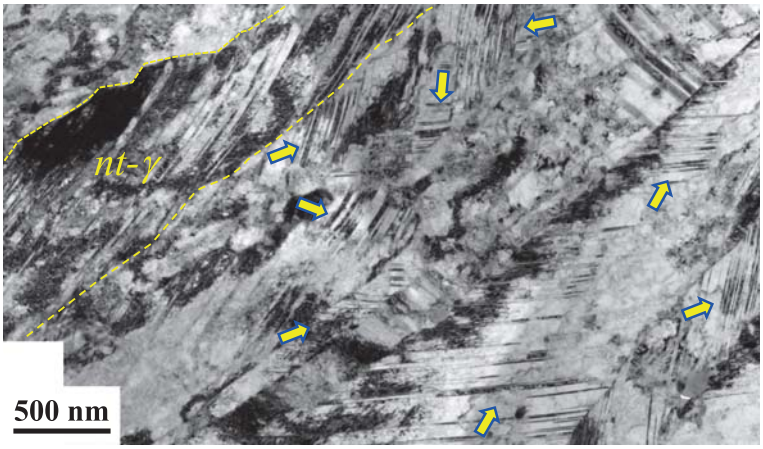

Fig. 11. A TEM image showing deformation twins formed in many grains in Region I (arrows) at a strain of 22%.

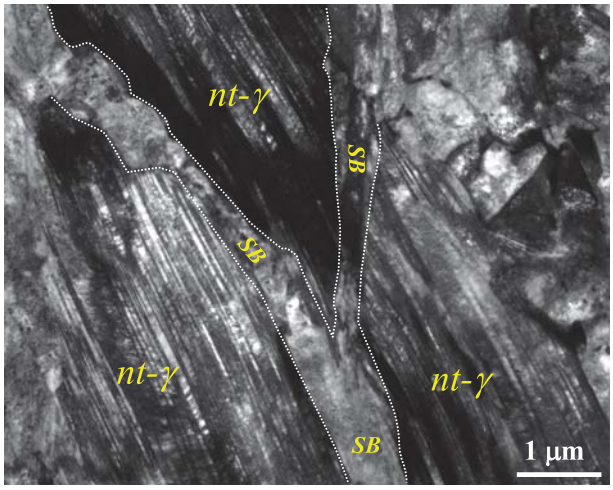

Fig. 12. A bright-field TEM image showing the formation of shear bands in the *nt*-γ grains at a strain of 22%.

$$\left(\frac{\partial\sigma}{\partial\varepsilon}\right)_{\dot{\varepsilon}} \leqslant \sigma$$

where σ and ε are the true stress and true strain, respectively, ongoing strain-hardening is required to postpone the onset of localized necking already during the early stages of tensile deformation. Generally, nanocrystalline and ultrafine-grained austenitic steels are not able to sustain a large uniform elongation (often less than ~2%) due to the abrupt decrease in the work-hardening rate [47]. However, *nt*-γ grains can significantly enhance the mechanical properties and contribute to the work-hardening potential of austenitic steels. Previous investigations [18,35] indicated that the yield strength of *nt*-γ grains can be as high as ~2.0 GPa but can yet reach ~5% uniform tensile strain. Therefore, nanotwinned 316L steels exhibit a superior strength–ductility combination when compared to micrograined 316L steels and as-DPD alloys. Obviously, the plastic co-deformation mechanism of the nanotwinned steels is associated to the work-hardening behavior of *nt*-γ grains. As shown in Fig. 15, we compare the work-hardening rates of the nanotwinned steel with a sample containing a similar average grain size but without *nt*-γ grains. After the elastic–plastic transition, the nanotwinned 316L

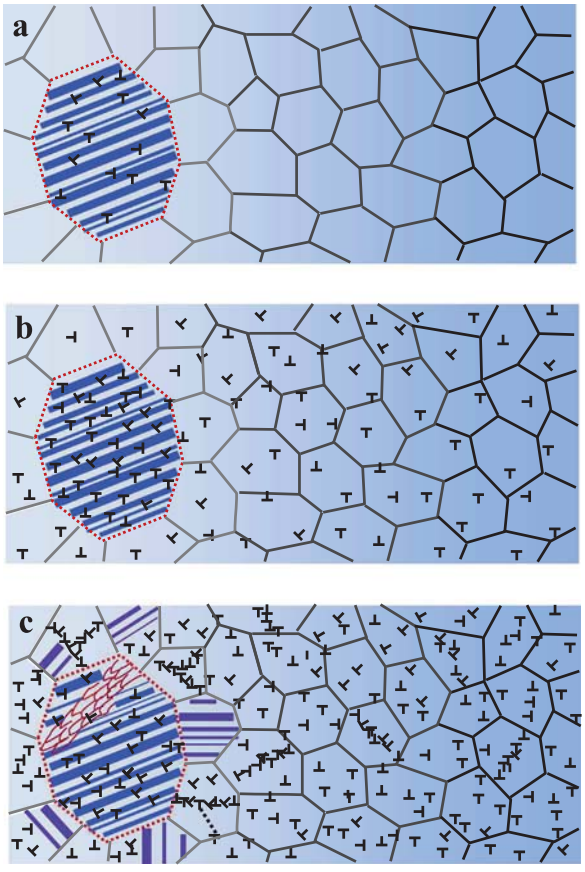

Fig. 13. A schematic illustration summarizing the plastic deformation mechanism of the austenitic steel strengthened by nanotwinned austenitic grains.

samples exhibit higher initial work-hardening rates ($\Theta = d\sigma/d\varepsilon$) than the micrograined samples. The two lines cross over at a strain of ~7%. As the global strain exceeds 7%, the work-hardening rate of the nanotwinned sample is lower than that of the *nt*-γ-free specimen. This value agrees with the observation that the *nt*-γ grains deform homogeneously together and are compatible with the softer SRX grains when the global strain is below 5%. The contributions of the SRX grains to the work-hardening rates might

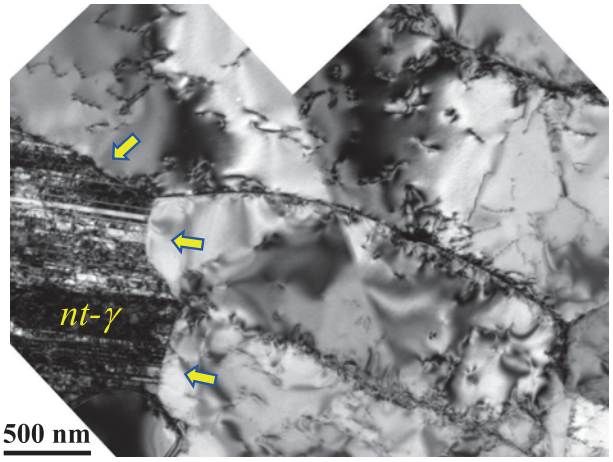

Fig. 14. A TEM image showing the interface between the *nt*-γ grain and the surrounding SRX grains at a tensile strain of 0.5%.

be comparable in the two samples. The higher initial work-hardening rate of the nanotwinned samples primarily originates from the *nt*-γ grains, which possess a very high initial work-hardening capability after annealing. Interactions of dislocations with TBs may generate glissile Shockley partials on the TBs [14,31]. The high density of TBs in the nanotwin bundles offers enough space for the motion of glissile partials and hence facilitates straining and work-hardening. With further straining, *nt*-γ grains cannot deform homogeneously and their work-hardening capability becomes exhausted. At this point, the less hardened SRX grains take over the overall work-hardening.

It is worth noting that the work-hardening behavior of the nanotwinned steel differs from that observed for the second-phase particle containing steels. In the latter case [9,48], the work-hardening rate is mainly determined by the density of GNDs around the hard phase [40,43,44]. Therefore, dual phase alloys work-harden much faster than single-phase materials, especially at initial strains of 1–2%. However, the work-hardening rate drops rapidly due to the extremely high dynamic recovery rate of stored dislocations around the hard phase. Hence, such materials cannot

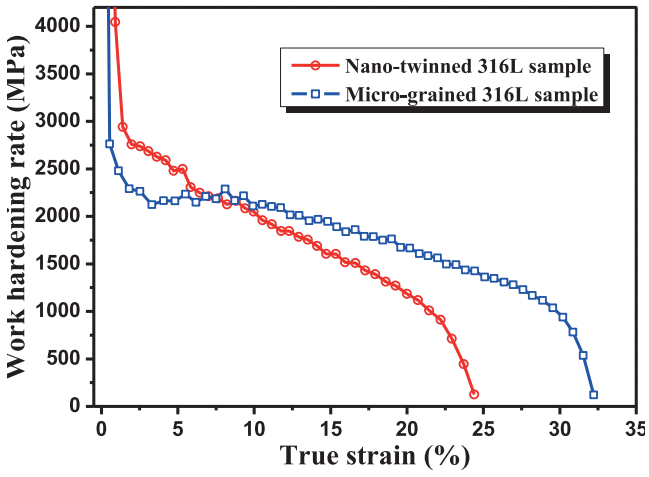

Fig. 15. Comparison of work-hardening rate vs. true strain between the nanotwinned 316L samples and the micrograined 316L samples.

sustain a high uniform strain owing to decohesion at the interfaces resulting from high stress/strain concentrations [39]. However, in nanotwinned steels, very high work-hardening rates are maintained in the initial plastic deformation regime until a global strain of 7%. Also, the work-hardening rates do not drop abruptly with ongoing loading as no significant strain gradient is developed and the elastically compatible homo-interfaces do not act as preferential sites for massive dislocation localization. These effects promote the uniform straining of such single-phase duplex microstructure steels and postpone damage initiation and fracture to higher strains.

5. Concluding remarks

We investigated the plastic deformation mechanisms of a novel type of single-phase duplex microstructure consisting of strong *nt*-γ grains embedded in soft SRX matrix grains in an 316L austenitic steel (X2CrNiMo19–12) by means of EBSD and TEM characterization. The *nt*-γ grains significantly strengthen the soft matrix. The two coexisting microstructures possess compatible elasticity. Two characteristic stages have been observed during uniaxial tensile deformation:

(i) Homogeneous deformation at small strains (below 5%) proceeds in a way that the *nt*-γ grains co-deform homogeneously with the surrounding microsized SRX grains without generating notable strain localizations at the interfaces between the two types of grains. The *nt*-γ grains can accommodate uniform plastic strain by slip and storage of dislocations. The anisotropic plastic deformation of the *nt*-γ grains results in a higher dislocation density in the SRX grains in the direction parallel to the TBs than that vertical to the TBs.

(ii) Inhomogeneous deformation at higher strains is characterized by a scenario in which localized deformation occurs within the *nt*-γ grains in the form of shear banding as the global tensile strains reach 12%. A strain gradient is developed inside the softer SRX grains as a function of the distance from the interfaces among the hard and soft crystals. Deformation twinning occurs in the SRX grains adjacent to *nt*-γ grains, while away from the *nt*-γ grains dislocation activities dominate the deformation of the SRX grains.

The rather low strain gradient generated from the strengthening *nt*-γ grains, in contrast to the high strain gradients induced by second-phase reinforcement in conventional steels, can explain satisfactorily the observed superior strength-ductility synergy in the *nt*-γ strengthened 316L steel. The *nt*-γ grains are very strong and ductile with high work-hardening rates at small strains. The *nt*-γ/SRX interfaces are not different from conventional austenite GBs and do not act as preferential sites for dislocation generation, hence do not promote strain localization. The strengthening effect associated with the *nt*-γ grains and the *nt*-γ/SRX interfaces accounts for the specific plastic co-deformation processes observed in this material. This concept of single-phase duplex microstructure steels offers a novel design path to the development of strong and yet ductile austenitic steels and related engineering alloys.

Acknowledgments

The authors are grateful for the financial support of the Ministry of Science and Technology of China (grant 2012CB932201) and the National Natural Science Foundation (grants 51371172, 51231006). The German Research Foundation (Deutsche Forschungsgemeinschaft DFG) is gratefully acknowledged for financial support through the project "SFB-761 – steel ab initio".

References

[1] F.B. Pickering, Physical metallurgy of stainless steel developments, Int. Met. Rev. 211 (1976) 227.
[2] X.H. Chen, J. Lu, L. Lu, K. Lu, Tensile properties of a nanocrystalline 316L austenitic stainless steel, Scr. Mater. 52 (2005) 1039.
[3] O. Bouaziz, Y. Brechet, J.D. Embury, Heterogeneous and architectured materials: A possible strategy for design of structural materials, Adv. Eng. Mater. 10 (2008) 24.
[4] R.G. Davies, Influence of martensite composition and content on properties of dual phase steels, Metall. Trans. A 9 (1978) 671.
[5] A. Bag, K. Ray, E. Dwarakadasa, Influence of martensite content and morphology on tensile and impact properties of high-martensite dual-phase steels, Metall. Mater. Trans. A 30 (1999) 1193.
[6] W. Xu, P.E.J. Rivera-Diaz-Del-Castillo, W. Yan, K. Yang, D. San Martin, L.A.I. Kestens, S. van der Zwaag, A new ultrahigh-strength stainless steel strengthened by various coexisting nanoprecipitates, Acta. Mater. 58 (2010) 4067.
[7] D. Raabe, D. Ponge, O. Dmitrieva, B. Sander, Nanoprecipitate-hardened 1.5 GPa steels with unexpected high ductility, Scr. Mater. 60 (2009) 1141.
[8] K. Lu, F.K. Yan, H.T. Wang, N.R. Tao, Strengthening austenitic steels by using nanotwinned austenitic grains, Scr. Mater. 66 (2012) 878.
[9] M.F. Ashby, Deformation of plastically non-homogeneous materials, Philos Mag. 21 (1970) 399.
[10] F.J. Humphreys, M.G. Ardakani, The deformation of particle-containing aluminum single-crystals, Acta. Metall. Mater. 42 (1994) 749.
[11] S. Ankem, H. Margolin, C.A. Greene, B.W. Neuberger, P.G. Oberson, Mechanical properties of alloys consisting of two ductile phases, Prog. Mater. Sci. 51 (2006) 632.
[12] D. Kurumlu, E.J. Payton, Ch. Somsen, A. Dlouhy, G. Eggeler, On the presence of work-hardened zones around fibers in a short-fiber-reinforced Al metal matrix composite, Acta. Mater. 60 (2012) 6051.
[13] L. Lu, Y.F. Shen, X.H. Chen, L.H. Qian, K. Lu, Ultrahigh strength and high electrical conductivity in copper, Science 304 (2004) 422.
[14] K. Lu, L. Lu, S. Suresh, Strengthening materials by engineering coherent internal boundaries at the nanoscale, Science 324 (2009) 349.
[15] X. Zhang, A. Misra, H. Wang, M. Nastasi, J.D. Embury, T.E. Mitchell, et al., Nanoscale-twinning-induced strengthening in austenitic stainless steel thin films, Appl. Phys. Lett. 84 (2004) 1096.
[16] B.Y.C. Wu, P.J. Ferreira, C.A. Schuh, Nanostructured Ni–Co alloys with tailorable grain size and twin density, Metall. Mater. Trans. A 36A (2005) 1927.
[17] Y.F. Shen, L. Lu, Q.H. Lu, Z.H. Jin, K. Lu, Tensile properties of copper with nano-scale twins, Scr. Mater. 52 (2005) 989.
[18] F.K. Yan, G.Z. Liu, N.R. Tao, K. Lu, Strength and ductility of 316L austenitic stainless steel strengthened by nano-scale twin bundles, Acta. Mater. 60 (2012) 1059.
[19] H.T. Wang, N.R. Tao, K. Lu, Strengthening an austenitic Fe–Mn steel using nanotwinned austenitic grains, Acta. Mater. 60 (2012) 4027.
[20] O. Bouaziz, D. Barbier, P. Cugy, G. Petigand, Effect of process parameters on a metallurgical route providing nanostructured single phase steel with high work-hardening, Adv. Eng. Mater. 14 (2012) 1.
[21] I. Gutierrez-Urrutia, D. Raabe, Dislocation and twin substructure evolution during strain hardening of an Fe–22 wt.% Mn–0.6 wt.% C TWIP steel observed by electron channeling contrast imaging, Acta. Mater. 59 (2011) 6449.
[22] I. Gutierrez-Urrutia, D. Raabe, Multistage strain hardening through dislocation substructure and twinning in a high strength and ductile weight-reduced Fe–Mn–Al–C steel, Acta. Mater. 60 (2012) 5791.
[23] Y.S. Li, N.R. Tao, K. Lu, Microstructural evolution and nanostructure formation in copper during dynamic plastic deformation at cryogenic temperatures, Acta. Mater. 56 (2008) 230.
[24] D. Raabe, Z. Zhao, S.J. Park, F. Roters, Theory of orientation gradients in plastically strained crystals, Acta. Mater. 50 (2002) 421.
[25] M. Calcagnotto, D. Ponge, E. Demir, D. Raabe, Orientation gradients and geometrically necessary dislocations in ultrafine grained dual-phase steels studied by 2D and 3D EBSD, Mater. Sci. Eng. A 527 (2010) 2738.
[26] G.E. Dieter, Mechanical Metallurgy, third ed., McGraw-Hill, New York, 1988.
[27] B.P. Kashyap, K. McTaggart, K. Tangri, Study on the substructure evolution and flow behavior in type 316L stainless steel over the temperature range 21–900 °C, Philos. Mag. A 57 (1988) 97.
[28] B.P. Kashyap, K. Tangri, On the Hall-Petch relationship and substructural evolution in type 316L stainless steel, Acta. Metall. Mater. 43 (1995) 3971.
[29] N.R. Tao, Z.B. Wang, W.P. Tong, M.L. Sui, J. Lu, K. Lu, An investigation of surface nanocrystallization mechanism in Fe induced by surface mechanical attrition treatment, Acta. Mater. 50 (2002) 4603.
[30] C.S. Hong, N.R. Tao, X. Huang, K. Lu, Nucleation and thickening of shear bands in nano-scale twin/matrix lamellae of a Cu–Al alloy processed by dynamic plastic deformation, Acta. Mater. 58 (2010) 3103.
[31] Z.H. Jin, P. Gumbsch, K. Albe, E. Ma, K. Lu, H. Gleiter, Interactions between non-screw lattice dislocations and coherent twin boundaries in face-centered cubic metals, Acta. Mater. 56 (2008) 1126.
[32] X.Y. Li, Y.J. Wei, L. Lu, K. Lu, H.J. Gao, Dislocation nucleation governed softening and maximum strength in nano-twinned metals, Nature 464 (2010) 877.
[33] Y. Zhang, N.R. Tao, K. Lu, Mechanical properties and rolling behaviors of nano-grained copper with embedded nano-twin bundles, Acta. Mater. (2008) 2429.
[34] F. Yan, H.W. Zhang, N.R. Tao, K. Lu, Quantifying the microstructures of pure Cu subjected to dynamic plastic deformation at cryogenic temperature, J. Mater. Sci. Technol. 27 (2011) 673.
[35] F.K. Yan, N.R. Tao, K. Lu, Tensile ductility of nanotwinned austenitic grains in an austenitic steel, Scr. Mater. 84–85 (2014) 31.
[36] Z.S. You, X.Y. Li, L.J. Gui, Q.H. Lu, T. Zhu, H.J. Gao, et al., Plastic anisotropy and associated deformation mechanisms in nanotwinned metals, Acta. Mater. 61 (2013) 217.
[37] T. Zhu, H.J. Gao, Plastic deformation mechanism in nanotwinned metals: An insight from molecular dynamics and mechanistic modeling, Scr. Mater. 66 (2012) 843.
[38] L. Zhou, G. Liu, X.L. Ma, K. Lu, Strain-induced refinement in a steel with spheroidal cementite subjected to surface mechanical attrition treatment, Acta. Mater. 56 (2008) 78.
[39] M. Calcagnotto, Y. Adachi, D. Ponge, D. Raabe, Deformation and fracture mechanisms in fine- and ultrafine-grained ferrite/martensite dual-phase steels and the effect of aging, Acta. Mater. 59 (2011) 658.

[40] M. Calcagnotto, D. Ponge, D. Raabe, Effect of grain refinement to 1 μm on strength and toughness of dual-phase steels, Mater. Sci. Eng. A 527 (2010) 7832.
[41] K. Konopka, J. Mizera, J.W. Wyrzykowski, The generation of dislocations from twin boundaries and its effect upon the flow stresses in FCC metals, J. Mater. Process. Technol. 99 (2000) 255.
[42] L. Lu, R. Schwaiger, Z.W. Shan, M. Dao, K. Lu, S. Suresh, Nano-sized twins induce high rate sensitivity of flow stress in pure copper, Acta. Mater. 53 (2005) 2169.
[43] J. Kadkhodapour, S. Schmauder, D. Raabe, S. Ziaei-Rad, U. Weber, M. Calcagnotto, Experimental and numerical study on geometrically necessary dislocations and non-homogeneous mechanical properties of the ferrite phase in dual phase steels, Acta. Mater. 59 (2011) 4387.
[44] D.A. Korzekwa, D.K. Matlock, G. Krauss, Dislocation substructure as a function of strain in a dual-phase steel, Metall. Trans. A 15 (1984) 1221.
[45] N.K. Balliger, T. Gladman, Work-hardening of dual-phase steels, Met. Sci. 15 (1981) 95.
[46] M.A. Meyers, O. Vohringer, V.A. Lubarda, The onset of twinning in metals: a constitutive description, Acta. Mater. 49 (2001) 4025.
[47] M.A. Meyers, A. Mishra, D.J. Benson, Mechanical properties of nanocrystalline materials, Prog. Mater. Sci. 51 (2006) 427.
[48] M.F. Ashby, Work hardening of dispersion-hardened crystals, Philos. Mag. 14 (1966) 1157.